Traveling-Wave Mach-Zehnder Modulator Integrated With Electro-Optic Frequency-Domain Equalizer for Broadband Modulation

Yuya Yamaguchi , *Member, IEEE*, Pham Tien Dat , *Member, IEEE*, Shingo Takano, Masayuki Motoya, Shotaro Hirata, Yu Kataoka, Junichiro Ichikawa, Satoshi Oikawa, *Member, IEEE*, Ryo Shimizu, Naokatsu Yamamoto, Kouichi Akahane, Atsushi Kanno , *Senior Member, IEEE*, and Tetsuya Kawanishi , *Fellow, IEEE*

Abstract—Broadband modulator is a key component of future high-capacity and high-baud-rate optical fiber communication. An electro-optic (EO) frequency-domain equalizer is proposed and investigated to increase the 3-dB bandwidth of optical modulators. The equalizer can be integrated with conventional traveling-wave modulators using a crossing waveguide, U-turn waveguide, or ferroelectric-domain-inversion. The 3-dB bandwidth of the modulator can be doubled by integrating the equalizer. As a theoretical consideration, we modeled several types of EO equalizers and investigated the function and parameter dependency of the equalizers in detail. For the experimental demonstration, a titanium-diffused lithium niobate optical waveguide modulator integrated with the EO equalizer was fabricated. The optical loss including fiber-coupling was as low as 5.4 dB, and the half-wave voltage was 3.7 V. The measured electro-optic response at 110 GHz is -0.4 dB, and that of the 3-dB bandwidth is larger than 110 GHz, which is the upper frequency limit of our measurement equipment. The 3-dB bandwidth of the modulator estimated using the fitting curve obtained from the measured electrical propagation loss of the modulator electrode was approximately 200 GHz.

Index Terms—Broadband modulation, high bandwidth, optical fiber communication, optical modulator.

I. INTRODUCTION

BROADBAND optical modulator is a key component of high-baud-rate optical links. Many techniques for signal

Yuya Yamaguchi, Pham Tien Dat, Naokatsu Yamamoto, and Kouichi Akahane are with the National Institute of Information and Communications Technology, Tokyo 184-8795, Japan (e-mail: yamaguchi@nict.go.jp; ptdat@nict.go.jp; naokatsu@nict.go.jp; akahane@nict.go.jp).

Shingo Takano, Masayuki Motoya, Shotaro Hirata, Yu Kataoka, Junichiro Ichikawa, Satoshi Oikawa, and Ryo Shimizu are with the Sumitomo Osaka Cement Co. Ltd., Chiba 274-8601, Japan (e-mail: stakano@soc.co.jp; mmotoya@soc.co.jp; shirata@soc.co.jp; ykataoka@soc.co.jp; jichikawa@soc.co.jp; soikawa@smt.soc.co.jp; rshimizu@soc.co.jp).

Atsushi Kanno is with the Nagoya Institute of Technology, Aichi 466-8555, Japan, and also with the National Institute of Information and Communications Technology, Tokyo 184-8795, Japan (e-mail: kanno.atsushi@nitech.ac.jp).

Tetsuya Kawanishi is with the Waseda University, Tokyo 169-8555, Japan, and also with the National Institute of Information and Communications Technology, Tokyo 184-8795, Japan (e-mail: kawanishi@waseda.jp).

Color versions of one or more figures in this article are available at https://doi.org/10.1109/JLT.2023.3266988.

Digital Object Identifier 10.1109/JLT.2023.3266988

multiplexing such as wavelength-division multiplexing (WDM) and space-division multiplexing (SDM) have been proposed and demonstrated to increase capacity of the optical fiber communication [1], [2]. Parallelization by multiplexing is promising owing to its scalability; however, the number of required optical devices increases depending on the number of parallelization. Increasing the modulation baud-rate can limit the number of required devices and overcome this issue. The bandwidth of the optical modulator is a significant parameter for converting electrical baseband signals into optical signals [3].

An optical modulator with a traveling-wave electrode is commonly used for broadband operation because its electrical bandwidth is limited not by the capacitance of the electrode, but by the RC time constant in the lumped electrode. In a traveling-wave modulator, the effective length of the modulation section can be large, and the half-wave voltage of the modulator becomes small. In general, traveling-wave electrode modulators have longer device lengths compared to lumped electrode modulators; hence, a material with low optical absorption is suitable for use as the substrate of the traveling-wave modulator.

Lithium niobate (LN) is a well-known material for modulators owing to its large nonlinear optical effect, and LN modulators are used commercially in optical fiber communication [4]. It features a large Pockels effect and low absorption in telecommunication optical wavelengths, which indicates low half-wave voltage and optical loss [5]. However, the dielectric constant at the microwave frequency is large, and the width of the signal electrode in a coplanar waveguide (CPW) must be sufficiently small to achieve impedance matching to 50 Ω. The electrical bandwidth of the optical modulator decreases owing to the large electrical propagation loss in the electrode. As a solution to this problem, research has been conducted on reducing the LN substrate thickness. The proposed concept involves replacing LN with another low-dielectric-constant material in the structure, except for the optical waveguide [6]. In the cross-sectional view, this is equivalent to reducing substrate thickness and bonding with a handling substrate made from a low-dielectric-constant material. Since the 2000s, several LN modulators with layered structures, whose LN layer is thinned to $\sim 10~\mu m$ by mechanical polishing (or mechanical machining), have been reported [7], [8], [9], [10], [11], [12], [13]. In the next decade, thin-film

LN modulators (also called LN on insulators, LNOI) with an LN layer thickness of <1 μm have been reported owing to the development of smart-cut and crystal ion-slicing technologies [14], [15], [16], [17], [18]. In general, comparing the <10-μm thick LN modulator with a Ti-diffused optical waveguide and the <1-μm-thick thin-film LN modulator with a rib waveguide, the Ti-diffused modulators have lower optical loss. Conversely, the rib-waveguide thin-film LN modulator can achieve a lower half-wave voltage and larger 3-dB bandwidth. In theory, the optical loss on a thin-film LN, which consists of the propagation loss and coupling loss to optical fibers of the rib waveguide, can be as small as that in a Ti-diffused waveguide by optimizing the dry-etching process and integrating the spot-size converter [19], [20]. Moreover, several studies have been conducted on modulator structures, including device materials and layered substrates.

Although the layered structure of LN modulators has been investigated for over 20 years, the optical and electrical circuits have not changed much. Most optical amplitude (or intensity) modulators for digital coherent links have a Mach–Zehnder (MZ) interferometric waveguide and a traveling-wave electrode. Although several methods to decrease the electrical propagation loss in the traveling-wave electrode have been investigated, the bandwidth of the optical modulator is strictly limited by the electrical loss [21], [22].

To realize a larger bandwidth when we use a traveling-wave electrode with a certain electrical loss, we proposed and demonstrated an electro-optic frequency-domain equalizer (EO equalizer) [23]. The EO equalizer structure can be integrated easily with a conventional traveling-wave modulator, and it can flatten the frequency response. In this study, the detailed circuit model and design method of an EO equalizer are investigated. Numerical analysis has been used to propose different equalizer structures.

II. TRAVELING-WAVE MODULATOR

Optical modulators with a traveling-wave configuration are major components in broadband modulation, such as digital coherent transmission in optical fiber communications. In general, the bandwidth of a traveling-wave modulator is limited by the velocity mismatch and electrical propagation loss. The velocity matching between a lightwave and the modulation microwave becomes critical in a longer effective-length modulator, and the structure of the traveling-wave modulator is generally designed to meet the velocity matching condition. When there is perfect velocity matching and no electrical propagation loss, the frequency dependence of the half-wave voltage (or sensitivity) of the modulator is perfectly flat, and the 3-dB bandwidth becomes infinite. However, electrical loss is not negligible in actual devices, and the bandwidth is limited to a finite frequency. The electrical propagation loss α_e consists of conductive and dielectric losses, described by

$$\alpha_e \ (f) = \alpha_c \sqrt{f} + \alpha_d f \tag{1}$$

where f is the frequency, α_c is the coefficient of conductive loss, and α_d is the coefficient of dielectric loss. As can be
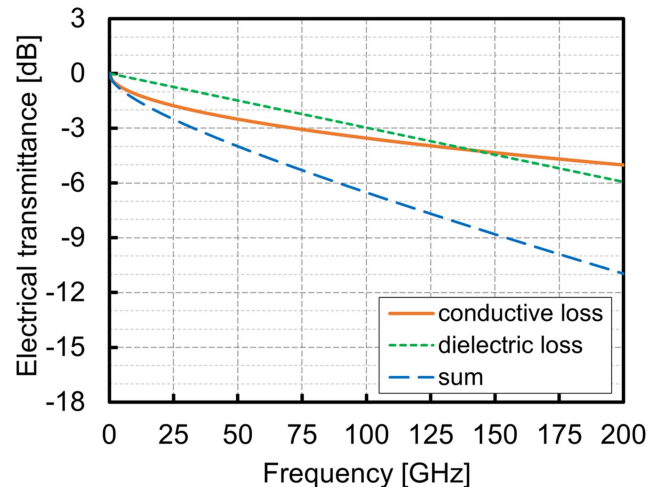

Fig. 1.   Calculation example of electrical propagation loss of a traveling-wave electrode in an optical modulator.

seen from the equation, conductive and dielectric losses are dominant at low and high frequencies, respectively, even though the exact relationship depends on the value of each coefficient. A sample calculation for electrical loss is shown in Fig. 1. In the numerical calculation, we assumed a 1.9 cm-long traveling-wave electrode that has the same cross-sectional structure as described in Ref. [13]. In this example, the conductive loss is larger than the dielectric loss at a frequency <140 GHz. In the semi-log graph, the total loss curve corresponding to the low-frequency range shows that the conductive component is dominant. The plot becomes straight in the high-frequency range where the dielectric loss is dominant.

Owing to the increase in the electrical propagation loss at high frequencies, the sensitivity of the traveling-wave modulators decreases in the high-frequency range, and the 3-dB bandwidth is limited. From this point of view, the reduction in both the conductive and dielectric losses is suitable for obtaining a large bandwidth. For example, a modulator with a copper electrode (instead of gold) is used to decrease the conductive loss, and a modulator with air cladding that is over- and under-clad by a membrane structure has been reported [11], [22].

III. ELECTRO-OPTIC FREQUENCY-DOMAIN EQUALIZER

The EO equalizer is proposed to maximize the 3-dB bandwidth of the traveling-wave modulator when the electrode has a finite electrical propagation loss. It enables the design of the frequency response of the modulator by optimizing the structural parameters of the equalizer. The device structure of a conventional MZ modulator with a push-pull configuration under null-bias conditions is shown in Fig. 2(a). The optical waveguides were positioned in the gap of the CPW electrode, and push–pull phase changes were applied to the lightwaves in the optical waveguides. Here, we assume an induced phase change of ϕ, and the optical transmittance in the electric field domain changes as $\sin \phi$, as shown in Fig. 2(b). The structure of the MZ modulator integrated with the EO equalizer is illustrated in Fig. 3(a). It consists of a fundamental modulation section, a same-polarity
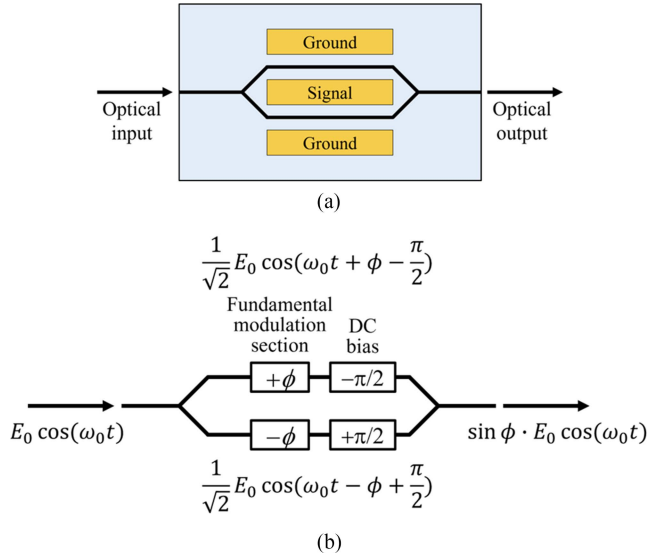
Fig. 2. (a) Structure of conventional traveling-wave MZ modulator in push–pull drive, (b) equivalent optical circuit of MZ modulator.
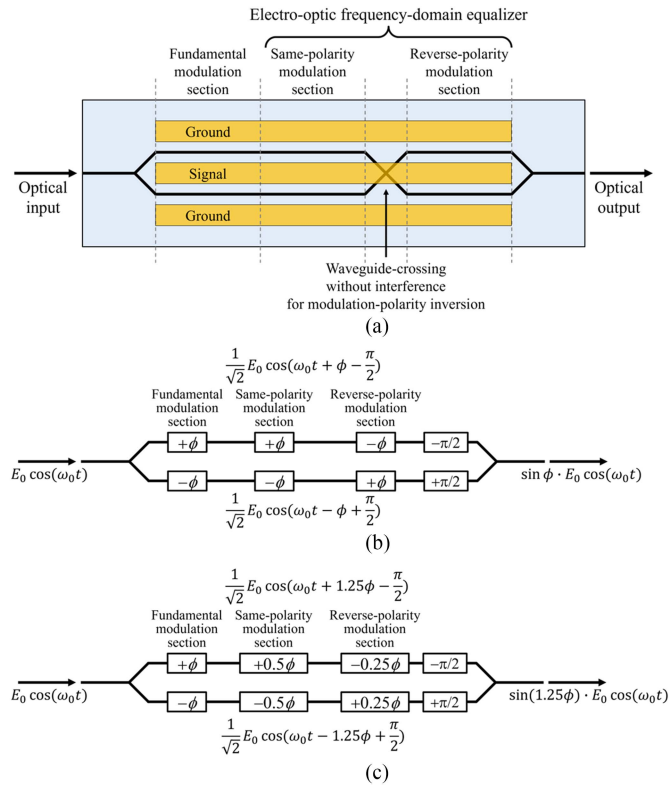

Fig. 3. (a) Structure of MZ modulator integrated with EO equalizer, (b) equivalent optical circuit in the case of loss-less electrode (e.g., low-frequency driving signal), (c) example of equivalent optical circuit in the case of high-frequency driving signal.

modulation section, a modulation polarity inversion section, and a reverse-polarity modulation section. In this case, the modulation polarity is reversed by exchanging the waveguide position using a crossing waveguide. The crossing waveguide is critical to optical switching devices; therefore, a method to design a low-loss and low-crosstalk crossing waveguide has been investigated
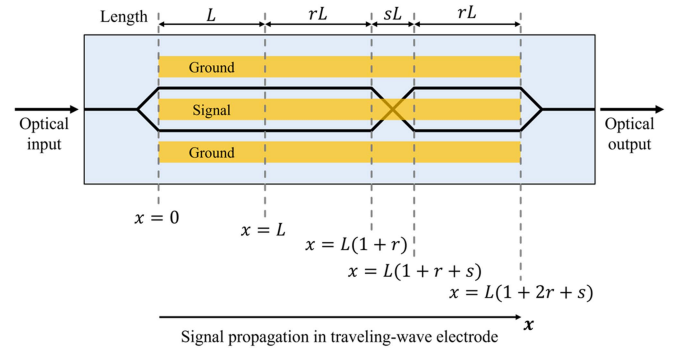

Fig. 4. Structural modelling and electrical signal propagation of a traveling-wave modulator integrated with EO equalizer.

[24]. The electrode differs from the conventional structure in terms of length, and hence, it is easy to integrate the EO equalizer with the conventional MZ modulator. The mechanism of the EO equalizer is shown in Fig. 3(b) and (c). In this case, it is assumed that the effective length of each modulation section is the same. When the driving signal has a low frequency, the electrical propagation loss is sufficiently small to be negligible. Then, the induced phase changes of the same-polarity modulation section and reverse-polarity modulation section cancel each other out perfectly. As a result, the summation of the induced phase change becomes ϕ as same as that of the conventional MZ modulator shown in Fig. 2(b). Conversely, the electrical propagation loss in the traveling-wave electrode is not negligible when the driving signal has a high frequency. Subsequently, the induced phase changes at the modulation section reduce with propagation. An example of an optical circuit in which the electrical voltage is halved by propagating the length of the fundamental modulation section is shown in Fig. 3(c). Owing to the electrical propagation loss, the induced phase changes at the modulation sections with identical and reverse polarities are not canceled out perfectly. Consequently, the total induced phase change of the high-frequency driving signal becomes larger than that of the low-frequency case. This indicates that the EO response in the high-frequency domain is improved by the EO equalizer, and the frequency response becomes flatter than conventional characteristics.

Here, we consider the mathematical modeling of the EO equalizer. The electro-optic circuit was modeled as shown in Fig. 4. The lengths of the fundamental modulation, same-polarity modulation, modulation polarity inversion (no-modulation), and reverse-polarity modulation sections are L, rL, sL, and rL respectively. The terms r and s refer to the ratios of the length of the modulation and non-modulation sections, respectively, in the EO equalizer compared to the fundamental modulation section. Then, the total length becomes $(1+2r+s)$ times that of the conventional modulator. The electrical voltage of the modulation signal is described as

$$V\ (x) = V_0 \exp\left\{-\alpha_e x\right\} \tag{2}$$

where V_0 is the amplitude of the input voltage signal α_e was defined in (1). In the conventional MZ modulator, the optical

phase change induced by the electro-optic effect is

$$\phi_{MZ} = \phi_0 \int_0^L V_0 \exp\{-\alpha_e x\}\, dx \tag{3}$$

where ϕ_0 is a coefficient that indicates the phase changes within unit length at the applied unit voltage. Conversely, the phase change in the MZ modulator integrated with the EO equalizer is described as follows.

$$\phi_{MZ\ with\ EQ} = \phi_0 \left[\int_0^{L(1+r)} V_0 \exp\{-\alpha_e x\}\, dx \right.$$
$$\left. - \int_{L(1+r+s)}^{L(1+2r+s)} V_0 \exp\{-\alpha_e x\}\, dx \right] \tag{4}$$

To compare the extent of the phase change, we define the ratio of the electro-optic response R_{EQ} as follows:

$$R_{EQ} \equiv \left| \frac{\phi_{MZ\ with\ EQ}}{\phi_{MZ}} \right|^2$$

$$= \left| \frac{\begin{array}{c} 1 - \exp\{-\alpha_e L(1+r)\} + \exp\{-\alpha_e L(1+r+s)\} \\ - \exp\{-\alpha_e L(1+2r+s)\} \end{array}}{1 - \exp\{-\alpha_e L\}} \right|^2 \tag{5}$$

As an example of a simple case, we assume $r = 1$ and $s = 0$. R_{EQ} is then calculated as a function of the frequency as follows:

$$R_{EQ}(f) = \left| \frac{1 - 2\exp\{-2\alpha_e(f)L\} + \exp\{-3\alpha_e(f)L\}}{1 - \exp\{-\alpha_e(f)L\}} \right|^2$$

$$= \left| 1 + \exp\{-\alpha_e(f)L\} - \exp\{-2\alpha_e(f)L\} \right|^2$$

$$= \left| -\left\{ \frac{1}{2} - \exp(-\alpha_e(f)L) \right\}^2 + \frac{5}{4} \right|^2 \tag{6}$$

The maximum R_{EQ} can be obtained at the frequency satisfying $\exp\{-\alpha_e(f)L\} = 1/2$, and the maximum value of $R_{EQ} = (5/4)^2 = 1.94$ dB regardless of the values of α_c, α_d, and L. However, the frequency where R_{EQ} is maximum depends on parameters α_c, α_d, and L, being calculable from (6). The frequency-dependent R_{EQ} is shown in Fig. 5. The horizontal axis represents the electrical loss in the power domain, which corresponds to the vertical axis in Fig. 1. Therefore, the horizontal axis also represents the frequency corresponding to the electrical propagation loss per fundamental modulation length L. In the case of a low frequency, the ratio of electro-optic response was ~0 dB. Conversely, R_{EQ} becomes 1.94 dB at a frequency whose electrical loss is 6 dB in the power domain. Because the frequency of the electrical $S_{21} \sim -6.4$ dB corresponds to the electro-optic $S_{21} \sim -3$ dB, the EO response at the frequency of the 3-dB bandwidth of the modulator was improved by 1.94 dB. An example of the numerical calculation of the relative EO response of the MZ modulator, with and without the EO equalizer, is shown in Fig. 6. The parameters of the electrical loss are the same as those shown in Fig. 1. In a conventional MZ modulator subjected to the velocity-matching condition, the electrical 6.4-dB bandwidth corresponds to the
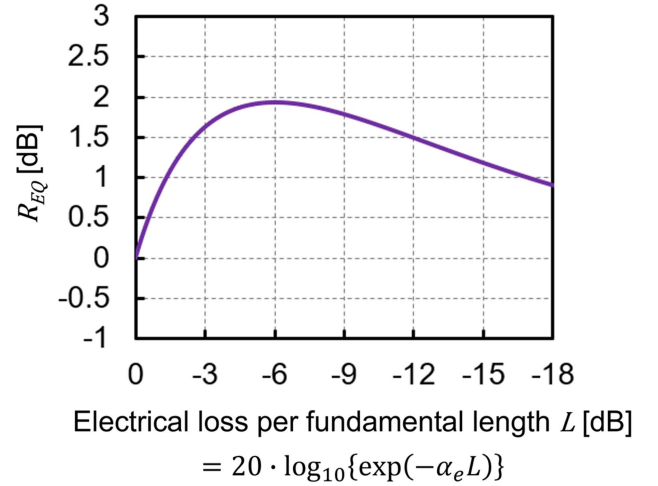

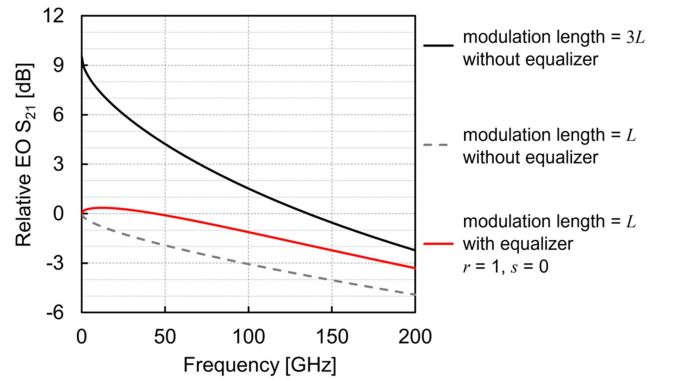Fig. 5. Ratio of electro-optic response R_{EQ} depending on the electrical loss.

Fig. 6. Numerical comparison on frequency response of the traveling-wave MZ modulator with and without EO equalizer.

electro-optic 3-dB bandwidth. In this case, the 6.4-dB electrical and 3-dB electro-optic bandwidths correspond to approximately 100 GHz. By integrating the EO equalizer, the EO response around 100 GHz was improved by 1.94 dB, and the 3-dB bandwidth became ~180 GHz. From an electrical loss point of view, the 3-dB electro-optic bandwidth corresponds to the 10.2-dB electrical bandwidth of the EO equalizer, whereas it corresponds to a 6.4-dB electrical bandwidth in a conventional traveling-wave modulator.

Next, we consider the relationship between the frequency response and the structural parameters r and s in the EO equalizer. As shown in Fig. 4, r and s are defined as the ratio of the lengths of the modulation section and non-modulation section in the EO equalizer, respectively, compared to the fundamental modulation section. The numerical calculation of the dependence of the frequency response on parameter r under the condition $s = 0$ is shown in Fig. 7. A larger 3-dB bandwidth can be obtained in the case of a larger r; however, the peak enhancement in the frequency range in the vicinity of 25 GHz also increases. For example, when $r = 1$, the over-enhancement in the frequency at approximately 10 GHz is less than 0.4 dB. Conversely, the peak EO response that occurs around 25 GHz is 2.7 dB when $r =$
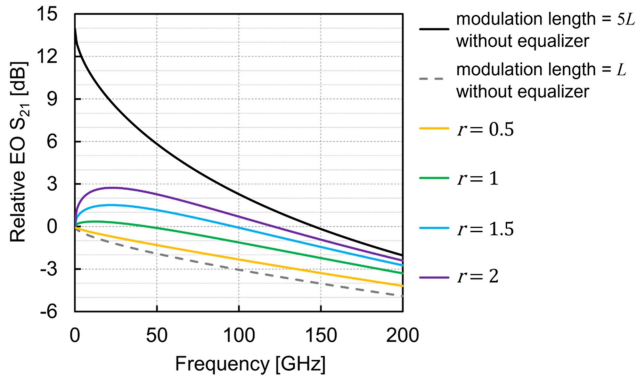
Fig. 7. Frequency response of the modulator integrated with EO equalizer depending on the parameter r under the condition of $s = 0$.
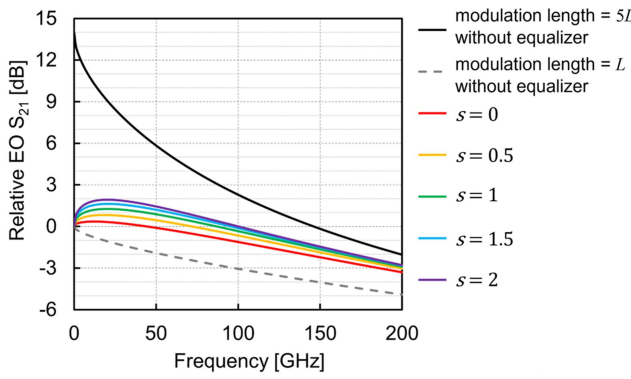

Fig. 8. Frequency response of the modulator integrated with EO equalizer depending on the parameter s under the condition of $r = 1$.
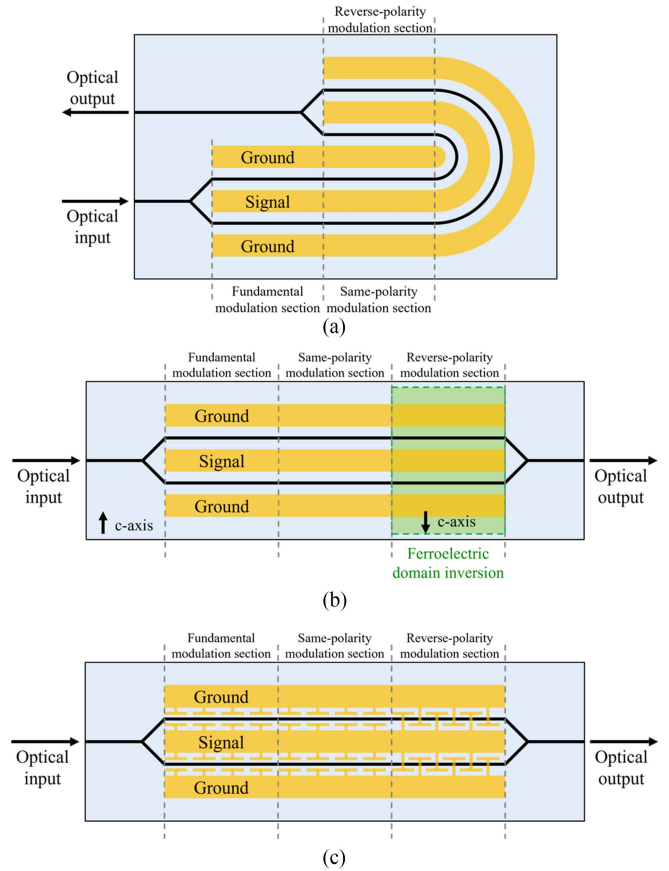

Fig. 9. Several types of EO equalizers: (a) U-turn waveguide type, (b) ferroelectric-domain-inversion type, (c) polarity-managed capacitively loaded electrode type.

2. Thus, the frequency response of the modulator can be customized by designing the parameter r to obtain the desired performance. For example, we can optimize parameter r to achieve the frequency response mask for high-bandwidth coherent driver modulators (HB-CDM) for commercial products standardized in OIF [25]. Next, we consider the equalizer parameter s. The relation between the ratio of the EO response R_{EQ} and s is shown in (5), and the dependency of the frequency response on the parameter s under the condition $r = 1$ is shown in Fig. 8. As in the case of r, a larger 3-dB bandwidth is obtained when the value of s increases because the waveguide-crossing section whose length is sL works as a low-selectivity low-pass filter attributed to the electrical propagation loss, which increases in higher frequency; the propagated low-frequency signals after the crossing section induces optical phase changes (or modulation) in the opposite direction compared to the fundamental modulation section. Therefore, a relatively higher EO response in the high frequency range can be obtained at larger s by suppressing the induced optical phase changes using high frequency signals in the reversed-polarity modulation section because the high frequency signals decrease when propagating the crossing section.

However, s indicates the length of the non-modulation section; therefore, the device length increases according to s, which is a disadvantage. In the crossing waveguide-type equalizer, s is

determined by the allowable bending radius of the optical waveguide in actual devices. The bending and crossing waveguides were designed to achieve a small additional loss attributed to the bending and crossing section, and the loss of the sum of the crossing and bending was estimated to <1 dB. The crossing waveguide was also designed to obtain a low optical crosstalk, and we estimated the crosstalk to <−30 dB from the analysis on the modulation distortions presented in Section V.

IV. SEVERAL TYPES OF EO EQUALIZER

In addition to the crossing waveguide-type EO equalizer, there are several other types of EO equalizers as shown in Fig. 9. The U-turn waveguide type EO equalizer is suitable for high-index-contrast waveguides, such as rib waveguides in thin-film LN modulators; the advantage of this type is that the device length may be reduced by the folded structure. In the ferroelectric-domain-inversion-type equalizer, modifying the structure of either the optical waveguide or the electrode is not necessary. This type requires an additional process of ferroelectric-domain inversion, but the polarization reversal of both bulk and thin-film LN is well established [26], [27]. The capacitively loaded traveling-wave electrode as a slow-wave electrode is a widely-used method for achieving velocity
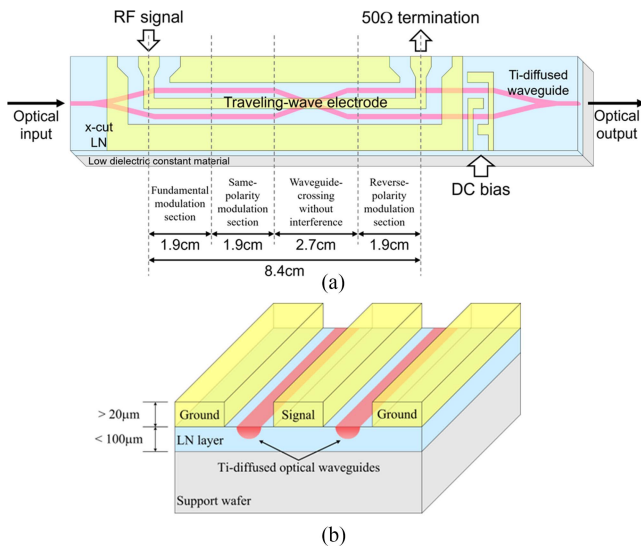
Fig. 10. (a) Structure of the Ti-diffused LN modulator integrated with crossing-waveguide-type EO equalizer, (b) cross-sectional structure at the modulation section.
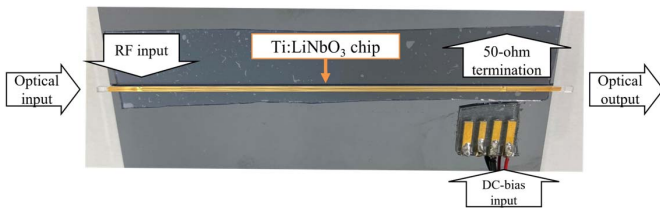

Fig. 11. Photograph of the device chip.

Fig. 12. Modulation curve of the fabricated MZ modulator.
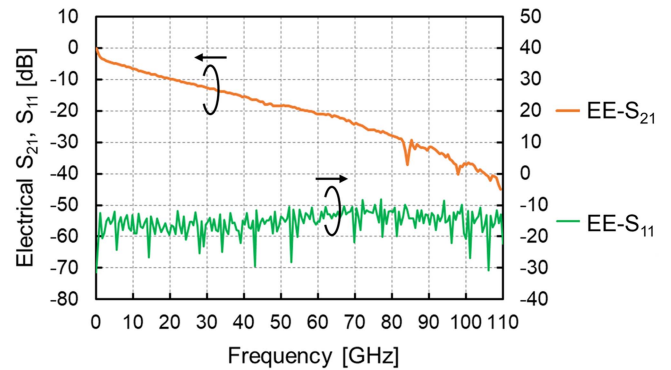
Fig. 13. Measured electrical S_{21} and S_{11}.

matching in thin-film LN modulators, and there is no need for structural modification of the optical waveguides.

V. EXPERIMENTAL DEMONSTRATION USING TI-DIFFUSED LN MODULATOR INTEGRATED WITH EO EQUALIZER

For the experiment, we fabricated a traveling-wave MZ modulator on a Ti:LiNbO$_3$ platform. The structure of the device is illustrated in in Fig. 10. We used an x-cut LN wafer as the substrate and formed an MZ-interferometric waveguide by the thermal diffusion of titanium. The traveling-wave electrode was formed by electroplating gold, and the electrode thickness was larger than 20 μm to reduce the electrical propagation loss. The width and gap of the electrode were chosen to satisfy the velocity-matching condition. To suppress the ripples in the frequency response owing to the mode coupling of the RF signals, the LN layer was thinned by polishing the back. The polishing also contributes to the reduction in the dielectric loss owing to the loss tangent of LN and the characteristic impedance matching to 50 Ω. As parameters of the EO equalizer, we set $r = 1$ and $s = 1.4$. The fundamental modulation length is 1.9 cm, and the total electrode length is 8.4 cm. In this case, s is designed to have a large value to reduce the bending loss of Ti-diffused waveguides to a negligible amount. To avoid optical absorption by the electrode at the waveguide crossing section, we inserted a buffer layer into the section. A photograph of the fabricated chip fixed to a handling Si wafer is shown in Fig. 11. A
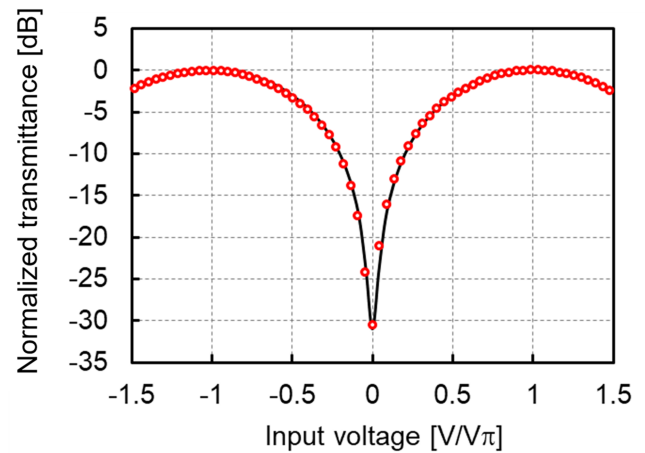
standard single-mode fiber is butt-coupled for the optical signal input to the chip, and we used RF probes with a 1-mm connector operating at up to 110 GHz for the electrical signal input. The optical insertion loss including the fiber-coupling loss was 5.4 dB, and the half-wave voltage (Vπ) was 3.7 V at ∼1 kHz frequency. The modulation curve is shown in Fig. 12. The extinction ratio was >30 dB and the modulation curve matched the theoretical sinusoidal function of the MZ modulator. We confirmed that the optical loss imbalance at the waveguide-crossing in the equalizer was small enough to achieve an extinction ratio of >30 dB and the optical crosstalk at the waveguide-crossing was estimated to <−30 dB from an analysis of the modulation distortions and modulation nonlinearity measurements.

The measured electrical S parameters are shown in Fig. 13. Electrical S_{21} decreased gradually as the frequency increased. This result is for an electrode of length 8.4 cm; when converted to a length of 1.9 cm, the result is in good agreement with the data shown in Fig. 1. The measured electro-optic S_{21} where the reference frequency was 10 MHz and its fitting curve are shown in Fig. 14. We confirmed that the 3-dB bandwidth of the fabricated modulator is larger than 110 GHz, which is the upper frequency limit of our measurement setup. Although the measured response fluctuated depending on the frequency, the response corresponding to 110 GHz after smoothing was only −0.4 dB. Thus, we realized an ultra-broadband modulator
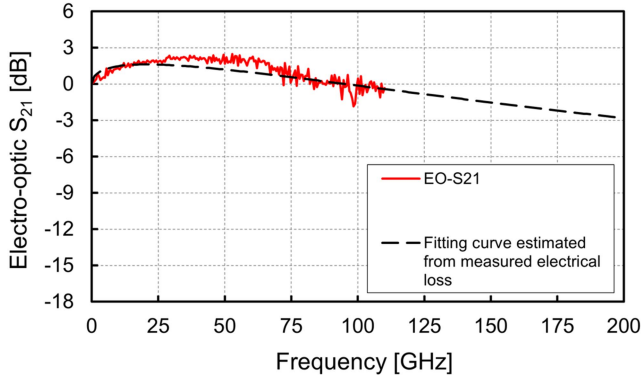
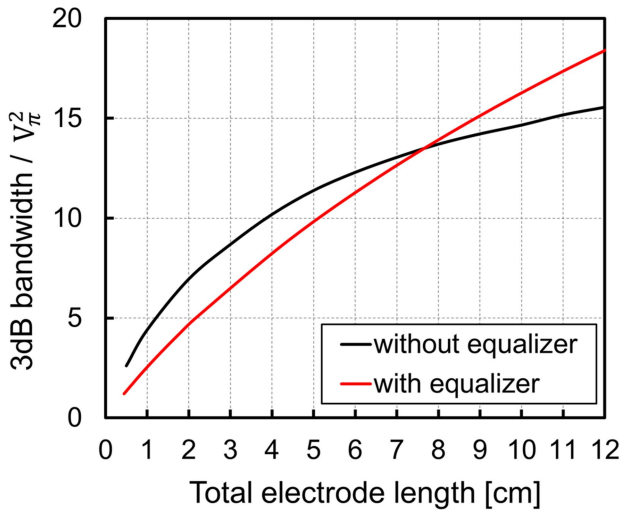Fig. 14. Measured electro-optic S_{21} (reference frequency = 10 MHz) and its fitting curve.

Fig. 15. The 3-dB bandwidth over V_π^2 product comparison of the modulator with and without EO equalizer under the same total electrode length condition (equalizer parameters: $r = 1$, $s = 1.4$). The modulator structure is assumed as same as our design.

of up to 110 GHz by integrating the EO equalizer. To estimate the 3-dB bandwidth, we calculated the electrical loss from the data in the <110 GHz range and added an extended fitting curve up to 200 GHz. We estimated that the device has the potential to operate at a high frequency in excess of 200 GHz.

As a future perspective, we will consider the relation between the modulator's performance and electrode length. Here, we define the product of the 3-dB bandwidth over V_π^2 as a figure of merit (FOM) [28], and then calculate the FOM of the modulators with and without the EO equalizer ($r = 1$, $s = 1.4$) under the same total electrode length condition, as shown in Fig. 15. The modulator structure is assumed to be similar to our design. In this case, the FOM can be increased by applying the proposed equalizer to the modulators with an electrode of > 7.7 cm. Because the electrode length of our modulator reported in this paper was 8.4 cm, we achieved better performance compared to that without the equalizer. Furthermore, although the FOM increased when the electrode length increased, the long-electrode modulator had a low half-wave voltage and low 3-dB bandwidth. For example, the half-wave voltage and 3-dB bandwidth

were estimated to 0.86 V and 10.4 GHz, respectively, in an 8.4-cm-electrode modulator without the equalizer in our design. Thus, increasing the electrode length is a simple and effective method to obtain a high FOM and to achieve a low half-wave voltage; however, the 3-dB bandwidth is limited to narrow. In the case of using the equalizer ($r = 1$, $s = 1.4$), the half-wave voltage and 3-dB bandwidth are estimated to 3.7 V and 202 GHz, respectively, in the 8.4-cm-electrode modulator consisting of the 1.9-cm fundamental modulation section, 1.9-cm same-polarity modulation section, 2.7-cm waveguide crossing-section, and 1.9-cm reversed-polarity modulation section. Thus, the combined use of the long-electrode and EO equalizer has a potential to maximize the performance or FOM of a traveling-wave modulator regardless of its cross sectional-structure.

VI. CONCLUSION

We proposed and investigated an EO equalizer that can improve the bandwidth of a traveling-wave optical modulator. We considered several EO equalizers with different structures, and numerical comparisons of their performance are described. As an experimental demonstration, we fabricated a Ti-diffused LN modulator integrated with an EO equalizer, and the measured 3-dB bandwidth was greater than 110 GHz. Furthermore, this equalizer can potentially be applied not only to Ti-diffused LN modulators, but also to thin-film LN, electro-optic polymers, and semiconductor-based modulators.

REFERENCES

[1] P. J. Winzer and D. T. Neilson, "From scaling disparities to integrated parallelism: A decathlon for a decade," *J. Lightw. Technol.*, vol. 35, no. 5, pp. 1099–1115, Mar. 2017.

[2] B. J. Puttnam, G. Rademacher, and R. S. Luis, "Space-division multiplexing for optical fiber communications," *Optica*, vol. 8, no. 9, pp. 1186–1203, Sep. 2021.

[3] X. Chen, G. Raybon, D. Che, J. Cho, and K. W. Kim, "Transmission of 200-GBaud PDM probabilistically shaped 64-QAM signals modulated via a 100-GHz thin-film LiNbO₃ I/Q modulator," in *Proc. Opt. Fiber Commun. Conf. Exhib.*, 2021, pp. 1–3.

[4] E. L. Wooten et al., "A review of lithium niobate modulators for fiber-optic communications systems," *IEEE J. Sel. Topics Quantum Electron.*, vol. 6, no. 1, pp. 69–82, Jan./Feb. 2000.

[5] A. A. Savchenkov, V. S. Ilchenko, A. B. Matsko, and L. Maleki, "Kilohertz optical resonances in dielectric crystal cavities," *Phys. Rev. A*, vol. 70, no. 5, Nov. 2004, Art. no. 051804.

[6] M. Izutsu, H. Haga, and T. Sueta, "Ultrafast travelling-wave light modulator with reduced velocity mismatch," in *Proc. Topical Meeting Picosecond Electron. Optoelectron.*, 1985, pp. 172–175.

[7] J. Kondo et al., "High-speed and low-driving-voltage thin-sheet X-cut LiNbO₃ modulator with laminated low-dielectric-constant adhesive," *IEEE Photon. Technol. Lett.*, vol. 17, no. 10, pp. 2077–2079, Oct. 2005.

[8] Y. Shi, "Micromachined wide-band lithium-niobate electrooptic modulator," *IEEE Trans. Microw. Theory Techn.*, vol. 54, no. 2, pp. 810–815, Feb. 2006.

[9] A. Kanno et al., "166Gb/s PDM-NRZ-DPSK modulation using thin-LiNbO₃-substrate modulator," in *Proc. Conf. Opt. Fiber Commun.*, 2010, pp. 1–3.

[10] V. E. Stenger et al., "Wide-band electro-optic modulator in thin-film lithium niobate on quartz substrate," in *Proc. 38th Eur. Conf. Exhib. Opt. Commun.*, 2012, pp. 1–3.

[11] J. Macario et al., "Full spectrum millimeter-wave modulation," *Opt. Exp.*, vol. 20, no. 21, pp. 23623–23629, Oct. 2012.

[12] Y. Yamaguchi, A. Kanno, N. Yamamoto, T. Kawanishi, and H. Nakajima, "High extinction ratio LN modulator with low half-wave voltage and small chirp by using thin substrate," in *Proc. Microoptics Conf.*, 2017, pp. 36–37.

[13] P. T. Dat et al., "Transparent fiber–radio–fiber bridge at 101 GHz using optical modulator and direct photonic down-conversion," in *Proc. Opt. Fiber Commun. Conf. Exhib.*, 2021, pp. 1–3.

[14] G. Poberaj, H. Hu, W. Sohler, and P. Gunter, "Lithium niobate on insulator (LNOI) for micro-photonic devices," *Laser Photon. Rev.*, vol. 6, no. 4, pp. 488–503, Feb. 2012.

[15] A. J. Marcante, S. Shi, P. Yao, L. Xie, R. M. Weikle, and D. W. Prather, "Thin film lithium niobate electro-optic modulator with terahertz operating bandwidth," *Opt. Exp.*, vol. 26, no. 11, pp. 14810–14816, May 2018.

[16] C. Wang et al., "Integrated lithium niobate electro-optic modulators operating at CMOS-compatible voltages," *Nature*, vol. 562, pp. 101–104, Sep. 2018.

[17] P. Kharel, C. Reimer, K. Luke, L. He, and M. Zhang, "Breaking voltage-bandwidth limits in integrated lithium niobate modulators using microstructured electrodes," *Optica*, vol. 8, no. 3, pp. 357–363, Mar. 2021.

[18] H. Mardoyan et al., "First 260-GBd single-carrier coherent transmission over 100 km distance based on novel arbitrary waveform generator and thin-film lithium niobate I/Q modulator," in *Proc. Eur. Conf. Opt. Commun.*, 2022, pp. 1–4.

[19] C. Hu et al., "High-efficient coupler for thin-film lithium niobate waveguide devices," *Opt. Exp.*, vol. 29, no. 4, pp. 5397–5406, Feb. 2021.

[20] M. Zhang, C. Wang, R. Cheng, A. Shams-Ansari, and M. Loncar, "Monolithic ultra-high-Q lithium niobate microring resonator," *Optica*, vol. 4, no. 12, pp. 1536–1537, Dec. 2017.

[21] J. Shin, S. R. Sakamoto, and N. Dagli, "Conductor loss of capacitively loaded slow wave electrodes for high-speed photonic devices," *J. Lightw. Technol.*, vol. 29, no. 1, pp. 48–52, Jan. 2011.

[22] Y. Zhang et al., "Systematic investigation of millimeter-wave optic modulation performance in thin-film lithium niobate," *Photon. Res.*, vol. 10, no. 10, pp. 2380–2387, Oct. 2022.

[23] Y. Yamaguchi et al., "Low-loss Ti-diffused LiNbO$_3$ modulator integrated with electro-optic frequency-domain equalizer for high bandwidth exceeding 110 GHz," in *Proc. Eur. Conf. Opt. Commun.*, 2022, pp. 1–4.

[24] K. Suzuki et al., "Low-loss, low-crosstalk, and large-scale optical switch based on silicon photonics," *J. Lightw. Technol.*, vol. 38, no. 2, pp. 233–239, Jan. 2020.

[25] OIF-HB-CDM-02.0 – Implementation Agreement for High Bandwidth Coherent Driver Modulator, Jul. 2021. [Online]. Available: https://www.oiforum.com/wp-content/uploads/OIF-HB-CDM-02.0.pdf

[26] L. E. Myers, R. C. Eckardt, M. M. Fejer, and R. L. Byer, "Quasi-phase-matched optical parametric oscillators in bulk periodically poled LiNbO$_3$," *J. Opt. Soc. Amer. B*, vol. 12, no. 11, pp. 2102–2116, Nov. 1995.

[27] C. Wang et al., "Ultrahigh-efficiency wavelength conversion in nanophotonic periodically poled lithium niobate waveguides," *Optica*, vol. 5, no. 11, pp. 1438–1441, Nov. 2018.

[28] M. Xu et al., "Dual-polarization thin-film lithium niobate in-phase quadrature modulators for terabit-per-second transmission," *Optica*, vol. 9, no. 1, pp. 61–62, Jan. 2022.

Yuya Yamaguchi (Member, IEEE) received the B.E., M.E., and Ph.D. degrees in applied physics from Waseda University, Tokyo, Japan, in 2012, 2014, and 2017, respectively. From 2015 to 2016, he was a Research Associate with Waseda University. Since 2016, he has been with the National Institute of Information and Communications Technology (NICT), Tokyo. His research interests include optical modulators and functional optoelectronic devices. Dr. Yamaguchi is a Member of the Institute of Electronics, Information, and Communication Engineers of Japan, and the Japan Society of Applied Physics.

Pham Tien Dat (Member, IEEE) received the B.Eng. degree in electronics and telecommunication engineering from the Posts and Telecommunications Institute of Technology, Hanoi, Vietnam, in 2003, and the M.Sc. and Ph.D. degrees in science from Waseda University, Tokyo, Japan, in 2008 and 2011, respectively. In 2011, he joined the National Institute of Information and Communications Technology, Tokyo, Japan, where he is currently a Senior Researcher. His research interests include microwave/millimeter-wave photonics, radio over fiber, optical wireless systems, and seamless access networks for 5G and beyond.

Shingo Takano received the B.E. and M.E. degrees in electronics from the Nagaoka University of Technology, Niigata, Japan, in 1998 and 2000, respectively. In 2000, he joined Optoelectronics Research Division, New Technology Research Laboratories, Sumitomo Osaka Cement Co., Ltd., Chiba, Japan. He has been engaged in research and development of optical modulators.

Masayuki Motoya received the B.E. and M.E. degrees in science and technology from Nihon University, Tokyo, Japan, in 2004 and 2006, respectively. In 2006, he joined Optoelectronics Research Division, New Technology Research Laboratories, Sumitomo Osaka Cement Co., Ltd., Chiba, Japan. He has been engaged in research and development of optical modulators.

Shotaro Hirata received the B.E. and M.E. degrees in applied chemistry from Osaka City University, Osaka, Japan, in 2016 and 2018, respectively. In 2018, he joined Optoelectronics Research Division, New Technology Research Laboratories, Sumitomo Osaka Cement Co., Ltd., Chiba, Japan. He has been engaged in research and development of optical modulators.

Yu Kataoka received the B.E. and M.E. degrees in chemistry and materials technology from the Kyoto Institute of Technology, Kyoto, Japan, in 2013 and 2015, respectively. In 2015, he joined Optoelectronics Research Division, New Technology Research Laboratories, Sumitomo Osaka Cement Co., Ltd., Chiba, Japan. He has been engaged in research and development of optical modulators.

Junichiro Ichikawa received the B.S. and M.S. degrees in mineralogy from the University of Tokyo, Tokyo, Japan, in 1987 and 1989, respectively. In 1989, he joined the Optoelectronics Division of Sumitomo Osaka Cement Co., Ltd. He has been engaged in research and development of ferroelectric material-based devices.

Satoshi Oikawa (Member, IEEE) received the B.E. and M.E. degrees in electrical engineering from Nihon University, Tokyo, Japan, in 1991 and 1993, respectively. In 1993, he joined Sumitomo Osaka Cement Co., Ltd., Chiba, Japan. He has been engaged in research and development of optical devices and optical systems.

Ryo Shimizu received the B.E. and M.E. degrees in electronics from Toyo University, Tokyo, Japan, in 1996 and 1998, respectively. In 1998, he joined Optoelectronics Research Division, New Technology Research Laboratories, Sumitomo Osaka Cement Co., Ltd., Chiba, Japan. He has been engaged in research and development of optical modulators.

Naokatsu Yamamoto received the Ph.D. degree in electrical engineering from Tokyo Denki University, Tokyo, Japan, in 2000. Since 2001, he has been with the Communications Research Laboratory (now the National Institute of Information and Communications Technology, NICT), where he is currently the Associate Director General of Photonic ICT Research Center, and also the Director of Advanced ICT Device Laboratory, NICT. He was also with Tokyo Denki University as a Visiting Professor in 2013 and the Ministry of Internal Affairs and Communications as the Deputy Director from 2012 to 2013. His research interests include quantum dot photonic devices, a heterogeneous integration technology for convergence of photonics and electronics and developing a novel optical and electrical frequency resource for a dedicated moderate range communication as an access network.

Kouichi Akahane received the B.E., M.E., and Ph.D. degrees in materials science from the University of Tsukuba, Tsukuba, Japan, in 1997, 1999, and 2002, respectively. He joined the Communications Research Laboratory (from April 1, 2004, National Institute of Information and Communications Technology), Koganei, Tokyo, in 2002. He is currently the Director of Optical Access Technology Laboratory, National Institute of Information and Communications Technology and is currently working on semiconductor photonic devices.

Atsushi Kanno (Senior Member, IEEE) received the B.Sci., M.Sci., and Ph.D. degrees in science from the University of Tsukuba, Tsukuba, Japan, in 1999, 2001, and 2005, respectively. In 2005, he was with the Venture Business Laboratory, Institute of Science and Engineering, University of Tsukuba. In 2006, he joined the National Institute of Information and Communications Technology (NICT), Japan. Since August 2022, he has been with the Nagoya Institute of Technology, Japan. His research interests include microwave photonics, broadband optical and radio communication systems, sensing applications, and automotive network technologies. Prof. Kanno is a Member of the Institute of Electronics, Information, and Communication Engineers, Japan Society of Applied Physics, Laser Society of Japan, SPIE.

Tetsuya Kawanishi (Fellow, IEEE) received the B.E., M.E., and Ph.D. degrees in electronics from Kyoto University, Kyoto, Japan, in 1992, 1994, and 1997, respectively. From 1994 to 1995, he was with the Production Engineering Laboratory, Panasonic. In 1997, he was with Venture Business Laboratory, Kyoto University, Kyoto, Japan, where he was engaged in research on electromagnetic scattering and near-field optics. In 1998, he joined the Communications Research Laboratory, Ministry of Posts and Telecommunications (now the National Institute of Information and Communications Technology), Tokyo, Japan. In 2004, he was a Visiting Scholar with the Department of Electrical and Computer Engineering, University of California at San Diego, San Diego, CA, USA. Since April 2015, he has been a Professor with Waseda University, Tokyo, Japan. His research interests include high-speed optical modulators and RF photonics. Prof. Kawanishi is the Chair of the Task Group on Fixed Wireless and Ground-Based Radar Systems (TG-FWS/GBRS) in Asia Pacific Telecommunity Wireless Group (AWG).